Applied Water Science (2023) 13:175
https://doi.org/10.1007/s13201-023-01987-2

ORIGINAL ARTICLE

Biosynthesis of magnesium oxide nanoparticles using *Hagenia abyssinica* female flower aqueous extract for characterization and antibacterial activity

Belete Yilma Hirphaye[1] · Nafikot Berhanu Bonka[1] · Alemu Mekonnen Tura[1] · Gada Muleta Fanta[1]

Received: 16 March 2023 / Accepted: 9 August 2023 / Published online: 19 August 2023

Abstract
The present study deals with the biosynthesis of magnesium oxide nanoparticles using the *Hagenia abyssinica* female flower aqueous extract. The prepared MgO NPs were characterized by visual observation, UV–Vis, XRD, FTIR, and SEM studies. Optimum parameters such as plant extract volume (25 mL), temperature (60 ℃), pH (12), precursor concentration (1 mM), reaction time (120 min), and the formation of the MgO NPs in the colloidal solution were monitored by a UV–Vis spectrophotometer. XRD patterns of MgO NPs confirmed the face-centered cubic structure and average crystallite size of NPs at 12.8 nm. The FTIR spectra depicted a peak at 407 cm^{-1}, which corresponds to the stretching vibration of MgO and is the characteristic peak for MgO NPs. SEM confirms spherical morphology, and the overall size of MgO NPs ranges from 10 to 40 nm. The antibacterial activity of synthesized MgO NPs was determined by the agar-well-diffusion method, which found that nanoparticles have significant antibacterial activity zone of inhibition against *Staphylococcus aureus* (27 ± 0.28 mm) and against *Escherichia coli* (15 ± 0 mm).

Keywords Biosynthesis · MgO NPs · *Hagenia abyssinica* · Morphology · Antibacterial activity

Introduction

Nanoscience and nanotechnology have been interesting fields of research and have gained much attention in the last three decades. A nanoparticle can be defined as a microscopic particle whose size falls between 1 and 100 nm (Amrulloh et al. 2021a, b, c; He et al. 2021; Fadaka et al. 2021).

It plays an essential role as a building block of nanotechnology. Nowadays, nanoscience as well as nanotechnology are widely applied in different fields, mainly in sensors, electronics, water purification, cosmetics, biomedical devices, pharmaceuticals, environmental remediation, catalysis, and material applications (Asadi et al. 2018). The size, crystallinity, and morphology of the nanomaterial can greatly influence its catalytic, magnetic, electronic, and optical properties (Cui and Lieber 2001).

NPs are synthesized through physical, chemical, and biological approaches (Gudikandula and Charya Maringanti 2016; Karimi and Ansari. 2018; Suresh et al. 2018). Recently, biosynthesis has become a popular way to produce NPs due to its low cost, environmental compatibility, workability in ambient conditions, and non-toxicity when compared to chemical and physical methods (Fatiqin et al. 2021). Plant extracts contain enzymes (including hydrogenases and reductases) and secondary metabolites such as flavonoids, terpenoids, phenols, and many other compounds that may react with metal salts to form precursors of metal oxide nanoparticles within a few minutes or hours (Amrulloh et al. 2021a, b, c; Suresh et al. 2018). Today, considerable interest is seen in the biosynthesis of different NPs as well as in evaluating their antibacterial activities (Gudikandula

✉ Gada Muleta Fanta
gadamuleta2019@gamil.com

Belete Yilma Hirphaye
y.belete2@gmail.com

Nafikot Berhanu Bonka
berhanunafkot066@gmail.com

Alemu Mekonnen Tura
kiyyach@gmail.com

[1] Department of Chemistry, College of Natural and Computational Sciences, Arba Minch University, Arba Minch, Ethiopia

and Charya Maringanti 2016; Ibrahim 2015; Prasanth et al. 2019; Yadav et al. 2017).

Owing to their ability to withstand harsh process conditions, inorganic materials, especially metals and metal oxides, have attracted a lot of attention over the last few decades (Asadi et al. 2018; Suresh et al. 2018). Magnesium oxide (MgO) is of particular interest because it is not only stable under difficult process conditions but is also regarded as a safe material for animals and humans (Stoimenov et al. 2002). MgO NPs have gained much interest in recent years due to their attractive properties, including unique ionic character, simple stoichiometry, crystal structure, surface structural defects, larger surface area-to-volume ratio, thermal and electrical properties, strong adsorption ability toward dye wastes and toxic gases, antimicrobial activity, non-toxicity, and biocompatibility (Bindhu et al. 2016; Bhagya et al. 2017; De-Silva et al. 2017). These also find extensive applications in catalysis, toxic waste remediation, paints, and superconducting devices. In addition, it is used in optical and electrical devices, including semiconductors. Its antibacterial properties are utilized in medicinal chemistry (Rao et al. 2014). Therefore, many authors report the successful synthesis of MgO NPs by using a biological method, and several plants are currently being investigated for their utility in the synthesis of MgO NPs. In this paper, the synthesis of MgO NPs using *H. abyssinica* female flowers is reported.

H. abyssinica (Bruce) Gmel. is a species of flowering plant native to the high elevation Afromontane regions of Central and Eastern Africa (Fig. 1). It is a multipurpose dioecious tree with separate female and male plants and is included in the family of Rosaceae (Azene et al. 1993). *H. abyssinica* has been used for centuries in Ethiopia and has great local importance. It is used locally for its medicinal properties; an infusion of dried female flowers is used to treat tapeworm; the roots are cooked with meat to make a soup for treating general illness and malaria; and the bark can be used to treat diarrhea and stomach aches (Desta 1995; Giday et al. 2003).

This work is aimed at the biosynthesis of MgO NPs using *H. abyssinica* female flower extract for characterization and antibacterial activity. The present approach has the advantage of easier work-up and cost-effectiveness. Also, this route is eco-friendly, and the conditions are milder without using any special equipment or high pressure or temperature. Characterization and antibacterial studies on the MgO NPs also were carried out.

Materials and methods

Chemicals

Chemicals used in this investigation include magnesium nitrate hexahydrate (98%, Mg $(NO_3)_2{\cdot}6H_2O$), hydrochloric acid (35.4%, HCl), and sodium hydroxide (98%, NaOH). Chemicals were used without further purification. The pH of the solution was adjusted by using 1 M of HCl and 1 M of NaOH.

Collection of plant

Fresh female flowers of *H. abyssinica* were collected from Dorze, Gamo Zone, SNNPR, Ethiopia, during the months of October to December, 2018. Identification of the plant species was confirmed with standard morphological characteristic features.

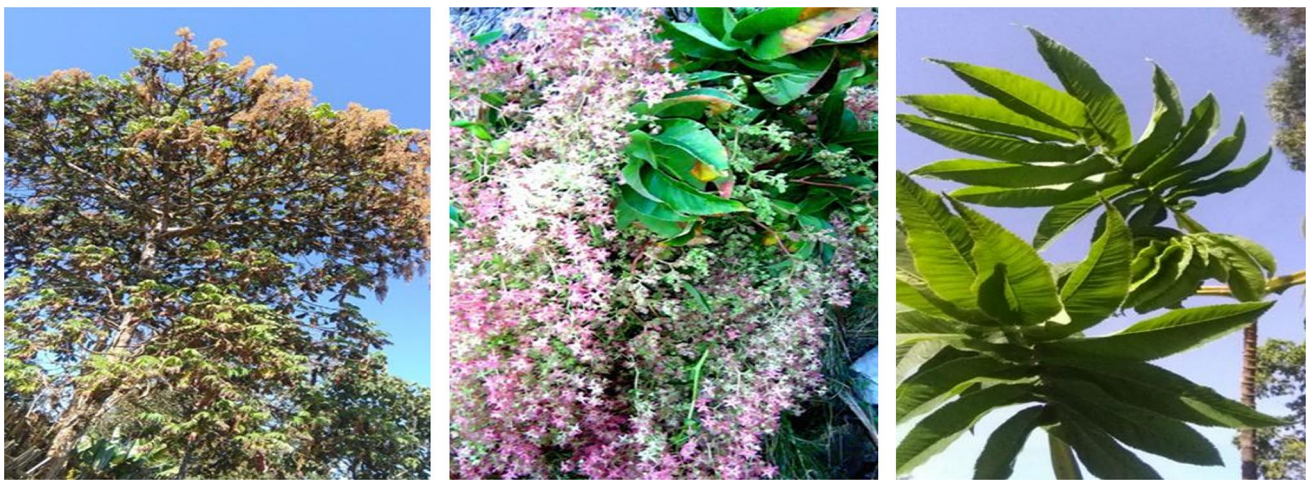

Fig. 1 Hagenia Abyssinica female flower

Test microorganisms

Two clinical microorganisms were collected from the Microbial Biotechnology Laboratory, Arba Minch University, Arba Minch, Ethiopia. The organisms used were: gram-negative bacteria (*E. coli*) and gram-positive bacteria (*S. aureus*). Both of these microorganisms were used for evaluating the antimicrobial efficiency of the synthesized NPs.

Plant extraction

The shade-dried flowers of *H. abyssinica* (at room temperature) were powdered using a mortar and pestle. Five grams of ultra-fine powder from *H. abyssinica* female flowers and 100 mL of deionized water were put into a 250-mL beaker. The mixture was heated at 100 °C on a hot plate for 30 min. Then, the extract was allowed to cool down to room temperature and filtered through filter paper (Whatman No. 1). The filtrate extract was stored at 4 °C for the next experiment.

Phytochemical screening test

The screening was carried out as per the standard methods. The extracts from *H. abyssinica* female flower were screened for the presence of naturally occurring biologically active compounds such as alkaloids, carbohydrates, proteins, tannins, phenols, saponins, flavonoids, terpenoids, steroids and glycosides. The screening was carried out as per the standard methods (Anantharaman et al. 2016; Amrulloh et al. 2021a, b, c).

Biosynthesis of MgO NPs using *H. abyssinica* flower extract

The biosynthesis of MgO NPs was performed after optimization of the synthesis parameters. Both *H. abyssinica* flower extract and magnesium nitrate hexahydrate solution were mixed in a 1:2 ratio and heated at 60℃ with constant stirring by a magnetic stirrer for 20 min to achieve the muddy brown solution in Fig. 2. The solution was then stirred for 2 h, while 1 M of NaOH was added drop by drop until the pH reached 12. The obtained solution was centrifuged and dried in an oven overnight at 60 ℃ and then calcinated at 500 ℃ for 3 h. Finally, the synthesized MgO NPs were stored for further characterization and application.

Effect of parameters on the biosynthesis of MgO NPs

The effects of the initial volume of *H. abyssinica* female flower aqueous extract (5–50 mL), precursor concentration (0.5–2.5 mM), reaction pH (2–12), temperature (30–200 °C), and heating time (30–240 min) were investigated and quantified spectrophotometrically in the 200–800 nm wavelength range. These parameters were varied one at a time, keeping all others constant.

Characterization

Biosynthesis of MgO NPs was confirmed by measuring the absorbance in UV–Vis spectra at a wavelength range of 200–800 nm. The powdered NPs samples were analyzed by XRD (Shimadzu, XRD-7000, Japan), FTIR (Shimadzu, IR Affinity-1S, Japan) and SEM (JSM-6390, Eindhoven, Netherlands). The average crystallite size, structure and phase of samples were determined by XRD with Cu$K\alpha$ radiation (Voltage = 40 kV, Current = 30 mA, $\lambda = 1.5406$ Å, scan speed 3.0 deg/min and scan range 2θ from 10 to 80 degrees). FTIR spectra were collected for both of *H. abyssinica* female flower aqueous extract and synthesized NPs. The spectra were obtained by employing potassium bromide (KBr) pellet method for the solid sample, while liquid sample was placed between two sodium chloride plates and the wavelength ranging from 400 to 4000 cm^{-1} was recorded. SEM reveals the morphological characteristics and distribution of the synthesized NPs.

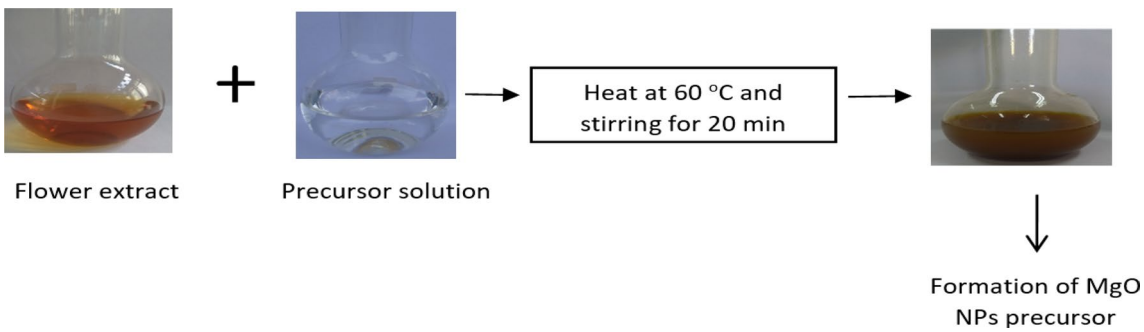

Fig. 2 Process flowcharts for the preparation of MgO NPs

Antimicrobial activity of MgO NPs

E. coli (gram-negative) and *S. aureus* (gram-positive) were maintained at 4 °C on broth media before use. A single colony of tested bacterial strain was grown overnight in a nutrient broth medium on a rotatory shaker at 200 rpm at 37 °C. 200 µL of freshly prepared culture and 700 µL of sterilized distilled water were taken through a micropipette and then mixed. Each diluted bacterial culture was uniformly spread on Muller-Hinton agar plates and left for 10 min for absorption. For spreading bacterial culture, sterile cotton swabs were used. The agar plates were punched for making wells of 6 mm in diameter for evaluating the antimicrobial activity of NPs using a sterilized cork borer. Four wells were made in each plate and then filled with 50 µL of various amounts (0.2, 0.4, 0.6, and 0.8 mg/mL) of synthesized MgO NPs. The antibiotic drug, chloramphenicol (30 µg), and sterile distilled water were used as positive and negative controls, respectively. The plates were then incubated for 24 h at 37 °C, where an inhibitory activity of NPs was observed as a clearing zone around the wells. The diameter of the clearing zone was measured in millimeter using the ruler scale.

Results and discussions

Phytochemical analysis

The phytochemical components of the *H. abyssinica* female flower were analyzed qualitatively for active compounds, and the results are given in Table 1. Aqueous extract of the plant flower showed the presence of phytochemically active compounds such as saponins, alkaloids, phenols, tannins, steroids, flavonoids, proteins and carbohydrate. But glycosides and terpenoids were absent. Aqueous flower extract exhibited the presence of saponins, alkaloids, phenols, tannins, steroids, flavonoids, proteins and carbohydrates. These bioactive compounds can serve as reducing, capping and stabilizing agents toward the synthesis of MgO NPs.

Table 1 Phytochemical analysis of *H. abyssinica* female flower aqueous extract

No	Phytochemical	Name of the test	Result
1	Saponins	Foam test	+
2	Alkaloids	Wagner test	+
3	Phenols	$FeCl_3$ test	+
4	Terpenoids	Chloroform test	−
5	Steroids	Chloroform test	+
6	Flavonoids	NaOH test	+
7	Glycosides	Salkowski's test	−
8	Tannins	KOH test	+
9	Proteins	Millon's test	+
10	Carbohydrate	Fehling's test	+

+ Present and − Absent

Optimization of synthesis parameters

Effect of volume of plant extract

Among different volumes of *H. abyssinica* female flower extracts, 25 mL yielded a higher proportion of MgO NPs at $\lambda_{max} = 267$ nm, as shown in Fig. 3a. This result is similar to the previously published studies (Jayarambabu et al. 2016). Absorbance increased with increasing the volume of aqueous flower extract from 15 to 25 mL. However, a further increase in the volume of flower extract resulted in a decrease in absorbance. Absorption was decreased with a higher volume of extract; this may be due to the presence of excess biomolecules in the plant's flowers. Therefore, 25 mL of extract volume is selected for the synthesis of MgO NPs.

Effect of temperature

On the basis of UV–Vis studies, 60 °C was found to be better for the synthesis of MgO NPs, as shown in Fig. 3b. This shows that the optimum temperature for a higher yield of NPs is 60 °C. The increase in absorbance increased with the increase in temperature (observed from 30 to 60 °C) and began to decline until it reached 200 °C. Temperatures above and below 60 °C led to lower yields of MgO NPs. Lower temperature is not sufficient for particle formation, and also higher temperatures degrade the active phytochemicals (Jeevanandam 2017). Similar temperature conditions were also used in synthesizing MgO NPs from plant extracts, in earlier studies (Jeevanandam et al. 2017).

Effect of pH

In our study, the solution was adjusted to different pH values (pH 2, 4, 6, 8, 10, and 12), and other parameters were kept constant. At neutral pH (i.e., pH 7), the reaction started as soon as the magnesium nitrate hexahydrate was added to the reaction medium. Reduction of Mg^{2+} ions was observed, which corresponds to the SPR peak at 267 nm. The highest absorption peak was at pH 12 in Fig. 3c, indicating the surplus formation of NPs. At pH 2–10, the absorbance peak observed was lower in comparison with pH 12, which indicates the poor degree of formation of NPs. Therefore, pH 12 was found to be effective for the synthesis of MgO NPs. Generally, alkaline pH was found to be optimum for the synthesis of NPs. Similar results were reported in the synthesis of MgO NPs using seeds and fruit waste (Ashwini et al. 2016; Jeevanandam et al. 2017).

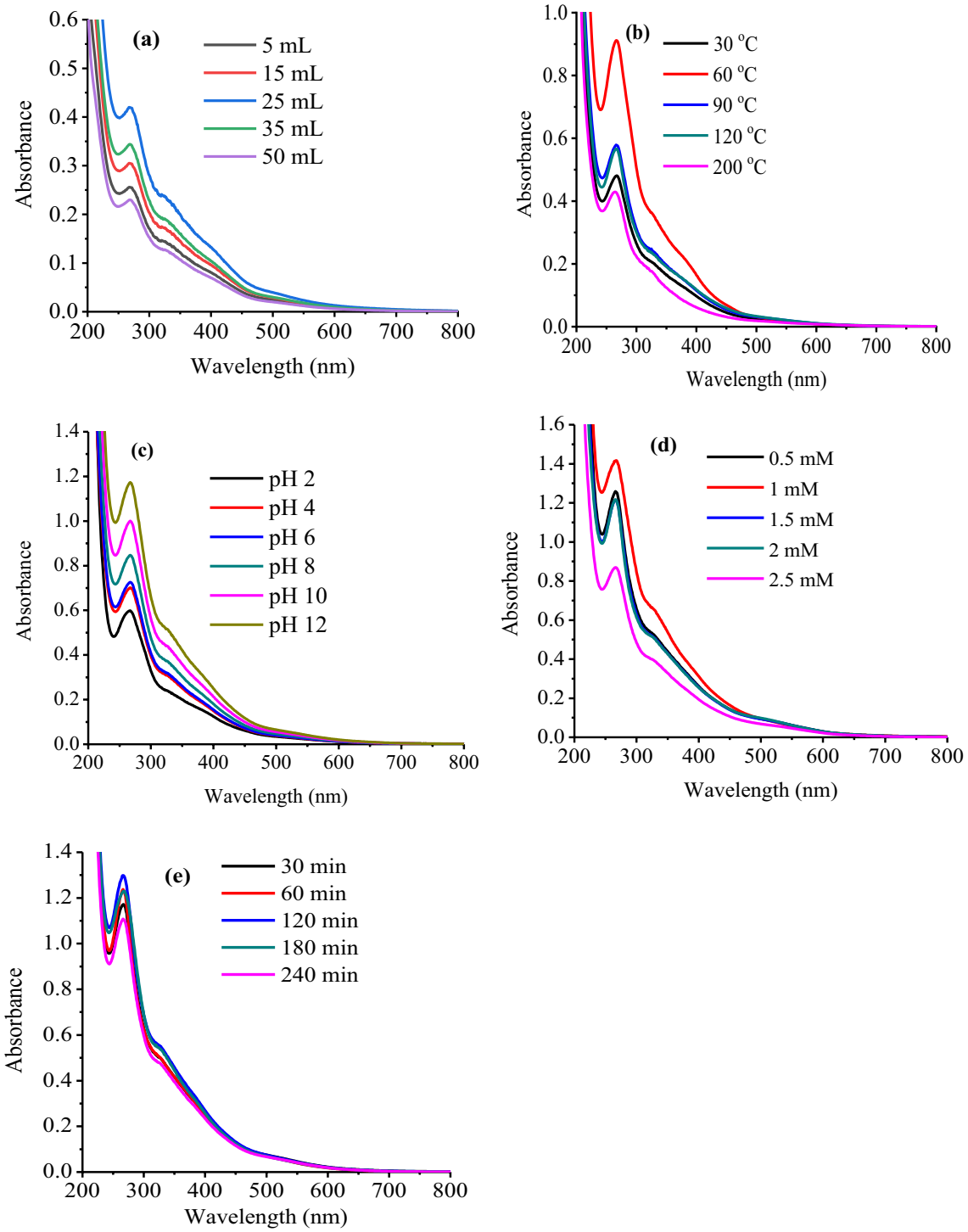

Fig. 3 Effective parameters on MgO NPs synthesis: **a** volume of flower extract, **b** temperature, **c** pH, **d** precursor concentration and **e** heating time

The unregulated nucleation and agglomeration at low pH, caused by enhanced interaction of negatively charged particles, can be attributed to the occurrence of larger NPs and platelets. On the other hand, in acidic pH, increased aggregation outdoes the nucleation process, while at alkaline pH, a greater number of nuclei formation instead of aggregation leads to the synthesis of more NPs with a smaller diameter (Anantharaman et al. 2016). Acidity suppresses the formation of NPs, but the basic conditions enhance their formation. This indicates that pH plays a

very important role in controlling the size and shape of MgO NP synthesis.

Effect of precursor concentration

Results of our study on the effect of metal salt solution showed that a 1 mM concentration of magnesium nitrate hexahydrate resulted in the formation of maximum nano-sized particles with an absorbance peak at 267 nm, as shown in Fig. 3d. The higher absorbance indicates a better yield of NPs. This result is in good agreement with the results of earlier investigations (Sharma et al. 2017).

The synthesis of NPs increased with the increase in magnesium nitrate hexahydrate concentration from 0.5 to 1 mM. Beyond this, there was again a fall in the absorbance. In this case, it was speculated that an increase in the magnesium nitrate concentration beyond 1 mM may yield more amounts of microparticles, but the characteristic absorbance of metal oxide NPs was poor at those higher precursor concentrations. Therefore, it can be depicted that metal ion concentration also plays a crucial role in NP formation.

Effect of heating time

Among various batches of varying heating times, the absorbance observed at 267 nm was the highest for the sample subjected to 120 min of heating time in Fig. 3e. UV–Vis absorbance increased gradually with increasing the heating time from 30 to 120 min and then began to decline until it reached 240 min. The size of NPs increased after the threshold time of heating (Jeevanandam 2017). Despite this, 120 min of heating time is selected as the optimum condition because it produces smaller NPs. Similar heating times were also applied in the biosynthesis of MgO NPs using mushroom extract (Jhansi et al. 2017).

Characterization of MgO NPs

Visual observation

Plant-mediated synthesis of MgO NPs is cost-effective, easily available, eco-friendly, and non-toxic, and there is no need to use high pressure, temperature, or energy, and also no requirement of cultural or isolation techniques for the performance of synthesis. In the preset study, the precursor is dissolved in deionized water, to which the flower extract is added under constant stirring, and the mixture is heated at 60 °C for 20 min. A color change from reddish brown to muddy brown was observed during the course of the reaction in Fig. 4. This change is caused by the coherent oscillation of electron gas at the surface of NPs, which results in surface plasma resonance (SPR) (Jayarambabu et al. 2016). The color change indicates the reduction of metal salts and hence corresponds to the successful synthesis of NPs (Sharma et al. 2017).

UV–Vis spectroscopy

Figure 5 shows the optical absorption of UV–Vis absorption of MgO NPs solution and initial aqueous extract of *H. abyssinica* female flower and magnesium nitrate solution. It was observed at a wavelength of 267 nm, which is in the range of 260–280 nm and is specific for MgO NPs. Similarly, MgO NPs synthesized using Trigonella foenum-graecum leaf extract (Vergheese and Kiran-Vishal 2018) showed very similar absorption peaks to bio-assisted MgO NPs. No

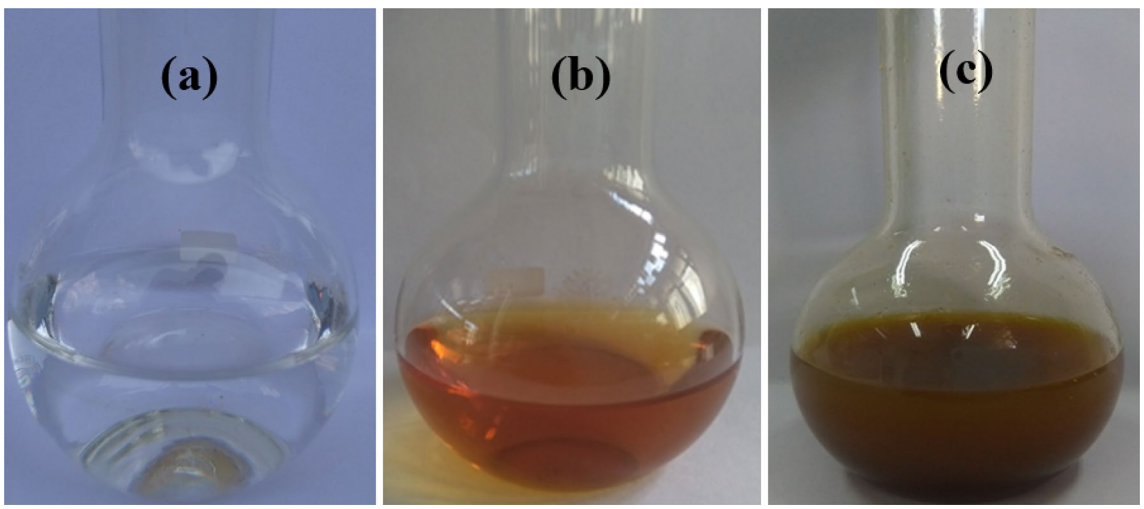

Fig. 4 Visual observation of MgO NPs synthesis **a** magnesium nitrate solution, **b** *H. abyssinica* female flower extract and **c** final color change in reaction mixture

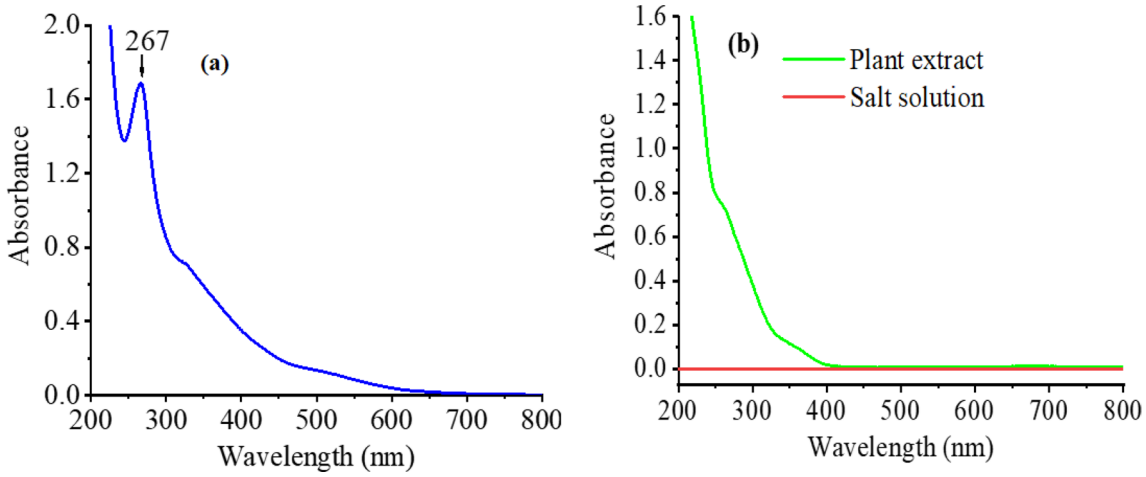

Fig. 5 UV–Vis absorption spectra of **a** final MgO NPs solution and **b** initial aqueous extract of *H. abyssinica* female flower and magnesium nitrate solution

other peaks were observed in the spectrum of synthetized NPs, which confirms the purity of MgO NPs.

A fundamental property of nanosized metal oxides is the bandgap energy. The band gap energy is the energy separation between the filled valence band and the empty conduction band (Moustafa et al. 2017). The energy bandgap can be estimated by assuming direct transmission between conduction and valance bands. From the optical absorption spectra, the direct optical bandgap was calculated (Alagesan and Venugopal 2019) using Equation: $(\alpha h\nu)^n = A(h\nu - E_g)$, where E_g = the energy gap, α = the absorption coefficient, h = Planck's constant, ν = the frequency of light, A = the constant of proportionality, and $n = 2$, for direct band gap energy. The energy bandgap (E_g) of synthesized nanoparticle can be obtained by plotting $(\alpha h\nu)^2$ versus photon energy ($h\nu$) and extrapolating the linear portion of the curve to the photon energy axis. The result revealed that the obtained energy bandgap of synthesized MgO NPs is 4.19 eV, from the extrapolation to linear line of the curve in Fig. 6. This is in close agreement with the previously published studies on *Citrus limon*, where the energy band gap was also 4.2 eV for MgO NPs (Haneefa 2017).

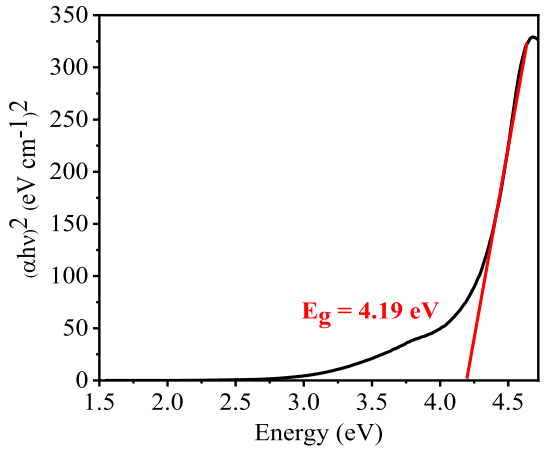

Fig. 6 Bandgap energy of MgO NPs synthesized

X-ray diffraction

X-ray diffraction (XRD) is a versatile, non-destructive analytical method for identification and quantitative determination of various crystalline forms present in powder and solid samples (Rao et al. 2014). Figure 7 represents the XRD patterns of the product obtained by calcination of the synthesized NPs precursor at 500 °C for 3 h. The sharp peaks of the synthesized MgO NPs clearly illustrate that the particles are highly crystalline. The interplanar spacing (d_{hkl} values), 2θ values and relative intensity values of MgO corresponding

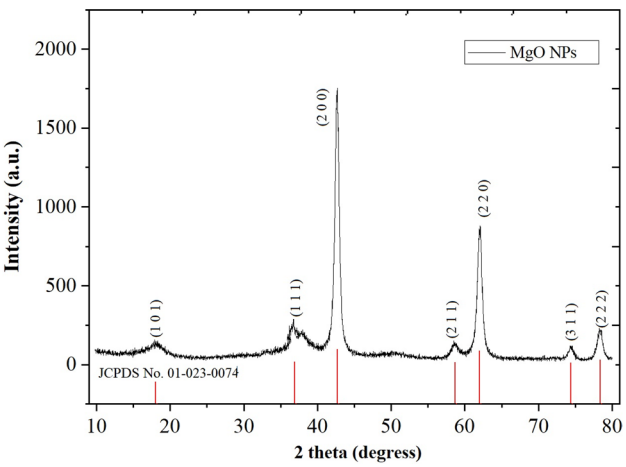

Fig. 7 XRD pattern of synthesized MgO nanoparticles

to the observed diffraction peaks were compared with the standard values of MgO (as reported by JCPDS-International Centre for Diffraction Data). XRD analysis showed a series of diffraction peaks at 2θ of 36.87°, 42.85°, 62.18°, 74.58° and 78.49° corresponding to the crystal planes of (111), (200), (220), (311) and (222), respectively, with no characteristic peaks corresponding to the impurities, which further confirms the formation of pure stable MgO phase. Stronger intense peak with 100% intensity belongs to (200) plane. As the width of the peak increases, size of particle decreases, reaching the order of nanorange. Confirmation of the results obtained is verified using the JCPDS standard XRD data (No: 01-023-0074).

The crystalline size of the synthesized MgO NPs was determined by using the Debye–Scherrer equation as follows:

$$D = \frac{k\lambda}{\beta \cos\theta}$$

where D = particle size of the crystal, k = Scherrer constant (usually 0.9), λ = wavelength of X-ray source, Cu$K\alpha$ radiation (1.5406 Å), β = full width at half-maximum (FWHM) of the diffraction peak in radian, and θ = Bragg's diffraction angle. The average crystalline size of MgO NPs calcined at 500 °C for 3 h was found to be 12.8 nm.

Fourier transforms infrared

Functional groups of possible bioactive molecules present in the *H. abyssinica* female flower extract, which act as reducing, capping, and stabilizing agents of synthesized MgO NPs, were identified using FTIR spectroscopy. Figure 8 shows that the changes in the intensity and small shifts were observed in the spectra of the *H. abyssinica* female flower extract and synthesized NPs. There are prominent absorption bands at 2330, 2093, 1654, 1427, 1061, 852, and 407 cm^{-1}. The spectra show an absorption peak at 2330 cm^{-1}, which indicates N–H stretching vibrations of secondary amine. The peak at 1654 cm^{-1} represents the stretching vibration of the N–H bond, while the peak observed at 2093 cm^{-1} corresponds to the C–C stretching vibration of polyol, carboxylic acid, ether, and ester. The absorption bands between 680 and 1454 cm^{-1} can be assigned to alcohols, phenolic groups, and the C–N stretching vibrations of amines (Kurniawan et al. 2021; Ratnani and Malik 2022). The absorption peak associated with the MgO stretching band clearly appears at 407 cm^{-1}, confirming the formation of MgO NP. The FTIR spectra of several MgO NPs samples synthesized using plant extracts have been demonstrated, and various MgO band positions appear at 610 cm^{-1} (Rahmani-Nezhad et al. 2017), 587–681 cm^{-1} (Fardood et al. 2018), 500–800 cm^{-1} (Palanisamy and Pazhanivel 2017),

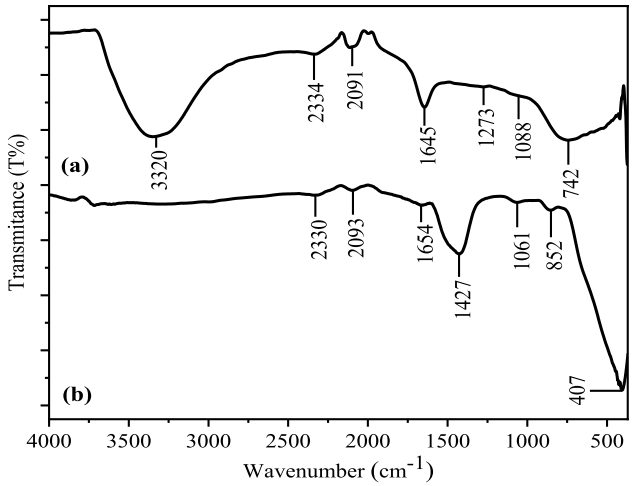

Fig. 8 FTIR spectra for **a** aqueous extract of *H. abyssinica* female flower and **b** synthesized MgO NPs

649.5–561.1 cm^{-1} (Jayarambabu et al. 2016), 419 cm^{-1} and 407 cm^{-1} (Dobrucka 2018). These results support our findings from the FTIR spectra of synthesized MgO NPs.

Scanning electron microscopy

Figure 9 shows the SEM image of synthesized NPs at different magnifications, such as X500, X1500, X3500, and X10000. The green-synthesized MgO NPs are spherical in shape and in the form of agglomerates, which may be due to the interactions and van der Waals forces between the particles (Sharma et al. 2017). The average particle size of MgO as seen in the SEM micrographs ranged from 10 to 40 nm. Similar results have been reported by another research group (Munja et al. 2017). Figure 10 shows the particle size distribution of the nanoparticles was estimated from the ImageJ software by treating the nanoparticles as spheres and thus calculating the particle size distribution from the deduced area.

Stability studies

The optimized as-prepared MgO NPs were kept as such in the dark at room temperature, and the stability of the synthesized NPs was monitored using UV–Vis spectral analysis by taking the spectra at different time intervals (1, 2, 3, 4, and 5 months). In the present study, there is no obvious change in color intensity, spectral peak position, or absorbance of NPs when monitored at regular intervals over a period of 5 months in Fig. 11. Greenly synthesized MgO NPs are uniform and stable, and they can be stored in the refrigerator for 5 months without any visible change. Stability of MgO NPs is much more important for applications (antimicrobial property). To attain greater stability and maximum yield

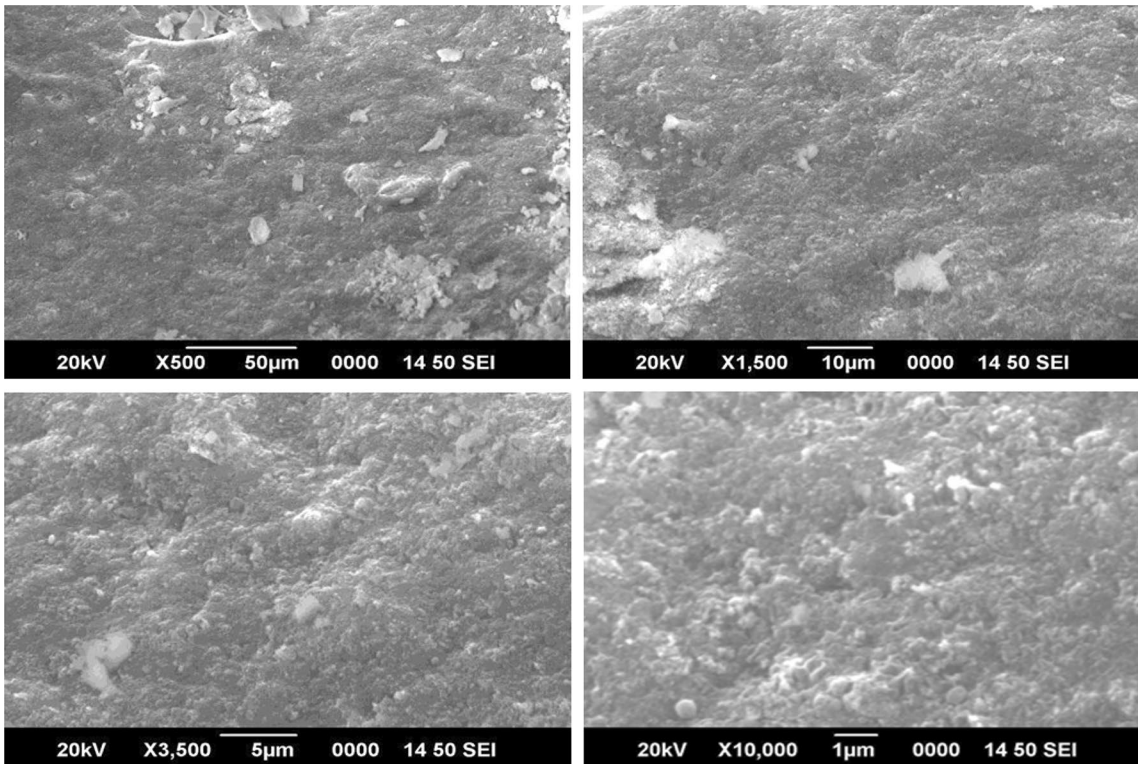

Fig. 9 SEM image of the synthesized MgO NPs

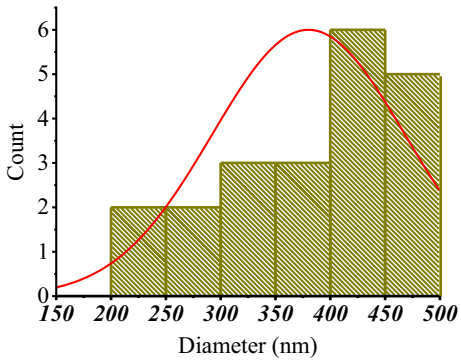

Fig. 10 Size distribution of MgO nanoparticles

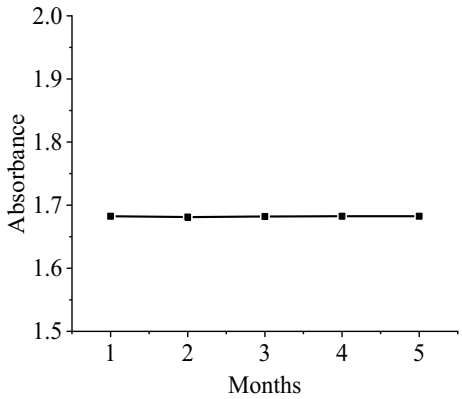

Fig. 11 Relation of absorption with MgO NPs solution at different time interval

with controlled size, it is imperative to optimize the different parameters used in the *H. abyssinica* female flower aqueous extract-mediated MgO NPs synthesis.

Antibacterial studies on MgO nanoparticles

E. coli and *S. aureus* are the most infectious agents of nosocomial diseases, besides having broad-spectrum antibiotic resistance due to the excessive use of antibiotics (Mahdy et al. 2017). Antibacterial activities of synthesized NPs are tested on both gram-positive (*S. aureus*) and gram-negative (*E. coli*) bacteria using the agar-well diffusion method. The results showed that green-synthesized MgO NPs demonstrated excellent antimicrobial activity against all tested strains. It has been found that the inhibition activity of NPs (0.8 mg/mL) against these microbial pathogens is high, and the ZID against *S. aureus* is 27 ± 0.28 mm, whereas the ZID value corresponding to chloramphenicol is 21 mm. On the other hand, the ZID

against *E. coli* was at 15 ± 0 mm, compared to the case of chloramphenicol, which has a value of 18.5 mm in Table 2.

Our results also revealed that the antimicrobial activity of synthesized MgO NPs increases as the quantity of NPs increases. In Fig. 12, it is shown that the zone of inhibition was found to be greater in gram-positive bacteria compared to gram-negative bacteria. A similar finding was reported by some authors, who found that the maximum bacterial effect on *S. aureus* is because of the easier interaction with these gram-positive bacteria, causing the distortion of the membrane structure of the bacteria's cell wall (Karthikeyan et al. 2016). In addition to this, gram-positive bacteria are characterized by having no outer membrane in the cell wall, and the thick cell wall is composed of multilayers of peptidoglycan. On the other hand, gram-negative bacteria have a more complex cell wall structure, with a layer of peptidoglycan between the outer membrane and the cytoplasmic membrane (Bindhu et al. 2016). Thus, the cell membrane of gram-positive bacteria can be damaged more easily. Previous inhibition results obtained are such that by Ibrahem et al. (2017), the values are 27 mm and 24 mm against *S. aureus* and *Pseudomonas aeruginosa*, respectively, for 1 mg/mL of MgO NPs, by Sundrarajan et al. (2012), the values are 23 mm and 21 mm against *S. aureus* and *E. coli,* respectively, for MgO NPs, and by Sharma et al. (2017), the values are also 17 mm and 18 mm against *S. aureus* and *E. coli,* respectively, for 0.25 µg/µL of MgO NPs, and we can report our obtained results have shown prominent activity.

Many studies report the ability of metal oxide NPs as an alternative to antibiotics due to the strong germicidal nature of the former. The antimicrobial mechanism of MgO NPs has been explained by a number of mechanisms, including the generation of ROS, an alkaline effect, and the interaction of NPs with bacteria and the subsequent damaging of the microbial cell (Tang and Lv 2014). Earlier authors propose that MgO NPs and bacteria interact in some way, leading to numerous antibacterial mechanisms (Cai et al. 2018). The NPs of MgO could strongly disrupt cell membranes essential functions of bacteria after the cells were exposed to suspensions of nanoparticle. In addition, the negatively charged pathogens are directly adhered to by the positively charged NPs. Firstly, the MgO NPs course ROS production or mechanical injure for damage cell wall and structure of membrane to initiate a leakage of cytoplasm in the cells. Then, the MgO NPs reduce the bacterial motility by inhibiting the aggregation of biofilms on the surface.

In addition, after permeating into the cells, the ROS could destroy DNA, eventually resulting in bacterial death. Ramanujam and Sundrarajan (2014) reported that the enhancement of the antimicrobial activity of MgO NPs against two pathogens (*S. aureus* and *E. coli*) was due to the decay of the outer membranes of bacteria by ROS (primarily ·OH), which cause cell death (Ramanujam and Sundrarajan 2014). It was reported that NPs that can directly contact the cell membrane of bacteria are bactericidal, and eventually the cell will die. The interaction of MgO NPs with bacteria, subsequently damaging the bacterial surface, has been proposed to explain the antimicrobial activity of MgO NPs. Suresh et al. (2013) suggested that MgO NPs inhibit the growth of microorganisms by using an electrochemical mode of action. When MgO NPs penetrate the cell wall, leakage of metabolites occurs and other

Table 2 Diameter of the inhibition zone of prepared MgO NPs

Tested bacteria	Diameter of zone of inhibition (in mm)				
	0.2 mg/mL	0.4 mg/mL	0.6 mg/mL	0.8 mg/mL	Control
S. aureus	14 ± 0.76	17 ± 0.86	20 ± 0.5	27 ± 0.28	21
E. coli	8 ± 0.25	10 ± 0.5	13 ± 0.86	15 ± 0	18.5

Control Chloramphenicol, mean zone inhibition (mm) ± standard deviation of three replicates

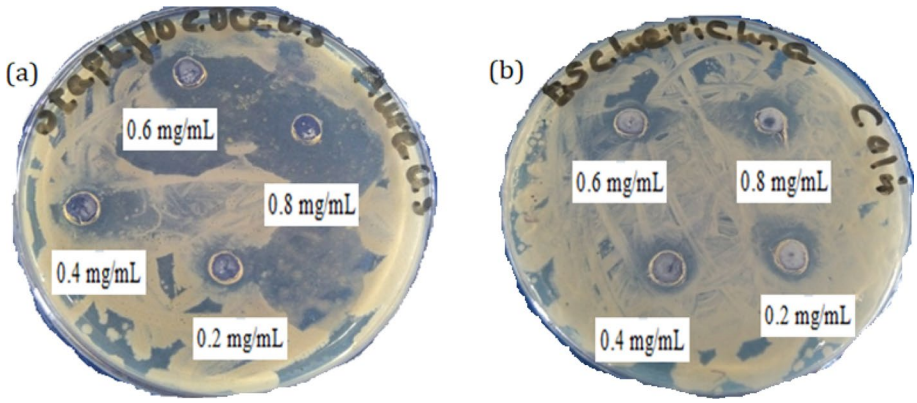

Fig. 12 Antibacterial activity (zone of inhibition): images of MgO nanoparticles against pathogen **a** *Staphylococcus aureus* and **b** *Escherichia coli*

Table 3 Comparison of antibacterial activity with other research studies

Metal oxide nanoparticles	Bacteria	Zone inhibition (mm)	References
MgO	*S. aureus*	27 ± 0.28	Present work
MgO	*E. coli*	15 ± 0	
MgO	*S. aureus*	27	Ibrahem et al. (2017)
MgO	*E. coli*	21	Ibrahem et al. (2015)
MgO	*S. aureus*	23	Sundrarajan et al. (2012)
MgO	*E. coli*	21	
MgO	*S. aureus*	17	Sharma et al. (2017)
MgO	*E. coli*	18	

cell functions are stopped, thereby preventing the organism from functioning or reproducing. Table 3 shows the comparison of antibacterial activity with other research studies.

Conclusions

It can be inferred from the current research that MgO nanoparticles were successfully synthesized using the green technique and female flowers of *H. abyssinica* as a reducing, capping, and stabilizing agent. The results obtained in this study show that MgO nanoparticles can be produced using *H. Abyssinica* female flower aqueous extract. Visual inspection, UV–Vis spectrophotometer, XRD, FTIR, and SEM were used to characterize the synthesized MgO nanoparticles studied for their optical and structural properties. The formation of MgO NPs is indicated by a color shift in the reaction mixture from reddish brown to muddy brown. The UV–Vis spectra of greenly synthesized MgO NPs revealed a peak at 267 nm. The SEM images show the formation of spherical-shaped NPs. The current study clearly reveals that the peak location and absorbance of MgO NPs at 267 nm do not change after 5 months, demonstrating that synthetic MgO NPs are highly stable. Greenly synthesized MgO NPs shown improved antibacterial efficacy against S. aureus and to a lesser extent *E. coli*.

Acknowledgements The authors acknowledge the laboratory facilities provided by Arba Minch University, College of Natural and Computational Sciences, Department of Chemistry.

Author contributions Conceptualization, AMT and GMF; investigation and data curation, NBB; writing—original draft, BYH and NBB writing—review and editing, AMT and GMF; supervision, BYH, AMT and GMF.

Funding There is no funding information, but we already acknowledged Arba Minch University for providing chemicals and apparatus.

Declarations

Conflict of interest The authors assert that the publication of this work is free of conflicts of interest.

Ethical approval This article does not contain any studies involving human, animal, or patient participants performed by any of the authors.

References

Alagesan V, Venugopal S (2019) Green synthesis of selenium nanoparticle using leaves extract of *Withania somnifera* and its biological applications and photocatalytic activities. BioNanoSci 9:105–116

Amrulloh H, Fatiqin A, Simanjuntak W, Afriyani H, Annissa A (2021a) Antioxidant and antibacterial activities of magnesium oxide nanoparticles prepared using aqueous extract of *Moringa oleifera* bark as green agents. J Multidiscip Appl Nat Sci 1:44–53

Amrulloh H, Kurniawan YS, Ichsan C, Jelita J, Simanjuntak W, Situmeang RT, Krisbiantoro PA (2021b) Highly efficient removal of Pb (II) and Cd (II) ions using magnesium hydroxide nanostructure prepared from seawater bittern by electrochemical method. Colloids Surf A 631:127687

Amrulloh H, Fatiqin A, Simanjuntak W, Afriyani H, Annissa A (2021c) Bioactivities of nano-scale magnesium oxide prepared using aqueous extract of *Moringa oleifera* leaves as green agent. Adv Nat Sci Nanosci Nanotechnol 12:015006

Anantharaman A, Sathyabhama S, George M (2016) Green synthesis of magnesium oxide nanoparticles using *Aloe vera* and its applications. Int J Sci Res Dev 4:109–111

Asadi S, Charati F, Akbari R, Razavi S (2018) Green synthesis of silver nanoparticles using *Taxus baccata* Leaves extract and identify its specifications. J Mater Environ Sci 9:2798–2803

Ashwini A, Sheethal K, Sathyabhama A, SMary G (2016) Green synthesis and its applications of magnesium oxide nanoparticles from the seeds of *Lepedium sativum*. Int J Recent Sci Res 7:14029–14032

Azene BT, Brinie A and Tegnäs B (1993). Useful trees and shrubs for Ethiopia identification, propagation and management for agricultural and pastoral communities. FAO of the United Nations. https://agris.fao.org/agris-search/search.do?recordID=ET19950156962

Bhagya J, Devadathan D, Baiju V, Biju R, Raveendran R (2017) Synthesis, characterization and photocatalytic activity of MgO nanoparticles. Int J Adv Res Sci Eng Technol 6:142–150

Bindhu MR, Umadevi M, Micheal MK, Arasu MV, Al-Dhabi NA (2016) Structural, morphological and optical properties of MgO nanoparticles for antibacterial applications. Mater Lett 166:19–22

Cai L, Chen J, Liu Z, Wang H, Yang H, Ding W (2018) Magnesium oxide nanoparticles: effective agricultural antibacterial agent against *Ralstonia solanacearum*. Front Microbiol 9:790

Cui Y, Lieber CM (2001) Functional nanoscale electronic devices assembled using silicon nanowire building blocks. Science 291:851–853

De-Silva RT, Mantilaka MMMPG, Goh KL, Ratnayake SP, Amaratunga GAJ, De-Silva KM (2017) Magnesium oxide nanoparticles reinforced electrospun alginate-based nanofibrous scaffolds with improved physical properties. Int J Biomater. https://doi.org/10.1155/2017/1391298

Desta B (1995) Ethiopian traditional herbal drugs. Part I: Studies on the toxicity and therapeutic activity of local taenicidal medications. J Ethnopharmacol 45:27–33

Dobrucka R (2018) Synthesis of MgO nanoparticles using Artemisia abrotanum herba extract and their antioxidant and photocatalytic properties. Iran J Sci Technol A 42:547–555

Fadaka A, Aluko O, Awawu S, Theledi K (2021) Green synthesis of gold nanoparticles using *Pimenta dioica* leaves aqueous extract and their application as photocatalyst, antioxidant, and antibacterial agents. J Multidiscip Appl Nat Sci 1:78–88

Fardood ST, Ramazani A, Joo SW (2018) Eco-friendly synthesis of magnesium oxide nanoparticles using Arabic gum. J Appl Chem 12:8–15

Fatiqin A, Amrulloh H, Simanjuntak W, Apriani I, Amelia RA, Syarifah S, Sunarti RN, Raharjeng AR (2021) Characteristics of nanosize MgO prepared using aqueous extract of different parts of Moringa oleifera plant as green synthesis agents. AIP Conf Proc 2331:040001

Giday M, Asfaw Z, Elmqvist T, Woldu Z (2003) An ethnobotanical study of medicinal plants used by the Zay people in Ethiopia. J Ethnopharmacol 85:43–52

Gudikandula K, Charya Maringanti S (2016) Synthesis of silver nanoparticles by chemical and biological methods and their antimicrobial properties. J Exp Nanosci 11:714–721

Haneefa MM (2017) Green synthesis characterization and antimicrobial activity evaluation of manganese oxide nanoparticles and comparative studies with Salicylalchitosan functionalized nanoform. Asian J Pharm 11:65–74

He YF, Chu DY, Zhuo Z (2021) Cycle stability of dual-phase lithium titanate (LTO)/TiO_2 nanowires as lithium battery anode. J Multidiscip Appl Nat Sci 1:54–61

Ibrahem EJ, Thalij KM and Badawy AS (2017) Antibacterial potential of magnesium oxide nanoparticles synthesized by *Aspergillus niger*. Biotechnol J Int 18:1–7

Ibrahim HM (2015) Green synthesis and characterization of silver nanoparticles using banana peel extract and their antimicrobial activity against representative microorganisms. J Radiat Res Appl Sc 8:265–275

Jayarambabu N, Kumari SB, Rao VK, Prabhu YT (2016) Enhancement of growth in maize by biogenic synthesized MgO nanoparticles. Int J Pure Appl Zool 4:262–270

Jeevanandam J, San-Chan Y, Danquah MK (2017) Biosynthesis and characterization of MgO nanoparticles from plant extracts via induced molecular nucleation. New J Chem 41:2800–2814

Jeevanandam J (2017) Enhanced synthesis and delivery of magnesium oxide nanoparticles for reverse insulin resistance in type 2 diabetes mellitus. Doctoral dissertation, Curtin University Australia 76–86.

Jhansi K, Jayarambabu N, Reddy KP, Reddy NM, Suvarna RP, Rao KV, Kumar VR, Rajendar V (2017) Biosynthesis of MgO nanoparticles using Mushroom extract: effect on peanut (*Arachis hypogaea* L.) seed germination. Biotech 7:263

Karimi EZ, Ansari M (2018) Comparison of antibacterial activity of ZnO nanoparticles fabricated by two different methods and coated on Tetron fabric. Open Biotechnol J 12:166–175

Karthikeyan V, Dhanapandian S, Manoharan C (2016) Characterization and antibacterial behavior of MgO-PEG nanoparticles synthesized via co-precipitation method. Int Lett Chem Phys Astron 70:33–41

Kurniawan YS, Priyangga KT, Krisbiantoro PA, Imawan AC (2021) Green chemistry influences in organic synthesis: a review. J Multidiscip Appl Nat Sci 1:1–12

Mahdy SA, Mohammed WH, Emad H, Kareem HA, Shamel R, Mahdi S (2017) The antibacterial activity of TiO_2 nanoparticles. J Univ Babylon 25:955–961

Moustafa IMI, Saleh IA, Abdelhami MR (2017) Synthesis of MgO nanoparticles from different organic precursors: catalytic decontamination of organic pollutants and antitumor activity. J Mater Sci Eng. https://doi.org/10.4172/2169-0022.1000359

Munja S, Singh A, Kumar V (2017) Synthesis and characterization of MgO nanoparticles by orange fruit waste through green method. Int J Adv Res Chem Sci 4:36–42

Palanisamy G, Pazhanivel T (2017) Green synthesis of MgO nanoparticles for antibacterial activity. Int Res J Eng Technol 4:137–141

Prasanth R, Kumar SD, Jayalakshmi A, Singaravelu G, Govindaraju K, Kumar VG (2019) Green synthesis of magnesium oxide nanoparticles and their antibacterial activity. Indian J Mar Sci 48:1210–1215

Rahmani-Nezhad S, Dianat S, Saeedi M, Hadjiakhoondi A (2017) Synthesis, characterization and catalytic activity of plant-mediated MgO nanoparticles using *Mucuna pruriens* L. seed extract and their biological evaluation. J Nanoanalysis 4:290–298

Ramanujam K, Sundrarajan M (2014) Antibacterial effects of biosynthesized MgO nanoparticles using ethanolic fruit extract of emblica officinalis. J Photoch Photobio B 141:296–300

Rao KG, Ashok CH, Rao KV, Chakra CS (2014) Structural properties of MgO nanoparticles: synthesized by co-precipitation technique. Int J Sci Res 3(12):43–46

Ratnani S, Malik S (2022) Therapeutic properties of green tea: a review. J Multidiscip Appl Nat Sci 2:90–102

Sharma G, Soni R, Jasuja ND (2017) Phytoassisted synthesis of magnesium oxide nanoparticles with *Swertia chirayita*. J Taibah Univ Sci 11:471–477

Stoimenov PK, Klinger RL, Marchin GL, Klabunde KJ (2002) Metal oxide nanoparticles as bactericidal agents. Langmuir 18:6679–6686

Sundrarajan M, Suresh J, Gandhi RR (2012) A comparative study on antibacterial properties of MgO nanoparticles prepared under different calcination temperature. Dig J Nanomater Bios 7:983–989

Suresh J, Gandhi RGR, Selvam S, Sundrarajan M (2013) Synthesis of magnesium oxide nanoparticles by wet chemical method and its antibacterial activity. Adv Mat Res 678:297–300

Suresh S, Pradheesh G, Ramani VA (2018) Biosynthesis and characterization of CuO, MgO and Ag_2O nanoparticles, anti inflammatory activity and phytochemical screening of the ethanolic extract of the medicinal plant *Pavetta indica* Linn. J Pharmacogn Phytochem 7:1984–1990

Tang ZX, Lv BF (2014) MgO nanoparticles as antibacterial agent: preparation and activity. Braz J Chem Eng 31:591–601

Vergheese M, Kiran-Vishal S (2018) Green synthesis of magnesium oxide nanoparticles using Trigonella foenum-graecum leaf extract and its antibacterial activity. J Pharmacogn Phytochem 7:1193–1200

Yadav J, Kumar S, Budhwar L, Yadav A, Yadav M (2017) Characterization and antibacterial activity of synthesized silver and iron nanoparticles using *Aloe vera*. J Nanomed Nanotechnol 7:2